

DEM–SPH Coupling Method for Landslide Surge Based on a GPU Parallel Acceleration Technique

Yu Zhang ^{a,b,*}, Shaohao Hou ^{b,**}, Shengjie Di ^c, Zaobao Liu ^a, Yifan Xu ^b

^a Key Laboratory of Ministry of Education on Safe Mining of Deep Metal Mines, Northeastern University, Shenyang, 110819, China

^b College of Pipeline and Civil Engineering, China University of Petroleum (East China), Qingdao 266580, China

^c Northwest Engineering Corporation Limited, Power China, Xi'an 710065, China



ARTICLE INFO

Keywords:
GPU parallel acceleration
G-DeSp
DEM–SPH coupling
Landslide surge
Solid–fluid interaction

ABSTRACT

A high-performance DEM–SPH coupling method for landslide surge is proposed based on a graphics processing unit (GPU) parallel acceleration technique. A GPU-based simulation program, namely, G-DeSp, is developed using C++ and Compute Unified Device Architecture language, which can simulate 3D landslide surge with millions of particles precisely and efficiently. A two-phase flow dam-break test is adopted to validate the accuracy and efficiency of G-DeSp. Three-dimensional landslide surge simulations are conducted with the different diameter of solid particles and the maximum climb height of the surge by granular slide and rigid slide is analyzed. Results show that G-DeSp accurately simulates landslide surge, such as the movement and deformation of the landslide, the generation and propagation of surge waves, and the violent interaction of the fluid–solid. The velocity and displacement of the granular slides and surge decrease with the increase in the diameter of solid particles. The maximum climbing height of surge by the rigid slide is 6.5 times that of surge by the granular slide with the same volume, which indicates that the surge hazard induced by the rigid slide is much more serious than that induced by the granular slide.

1. Introduction

Landslide surge is a frequent and serious geological disaster (Ren et al., 2023). The height of the surge provoked by landslides reaches tens to more than a hundred meters, and the climbing height on the opposite bank can reach hundreds of meters (Xu and Dong, 2021). These conditions result in serious damage to buildings at the reservoir and river bank. This incident leads to great casualties and property damage, such as the Lituya Bay landslide in the United States in 1958 (Fritz et al., 2001), Vajont reservoir landslide in Italy in 1963 (Panizzo et al., 2005), Qianjiangping landslide in China in 2003 (Yin et al., 2015), and Shuiyuba landslide in China in 2007 (Yin et al., 2008). Landslide surge is the process of rapid entry of geotechnical soil materials into the water to provoke a surge after the slope is destabilized, which contains complex solid–fluid interaction and dispersion of free surface flow in 3D space of large-scale propagation (Heller, 2007). Landslide collapse deformation impacts the water, which causes interactions of water and landslide body surface, and the transfer of kinetic energy (Fritz et al., 2003). The water and the landslide mass produce strong interactions, and this

phenomenon forms a fluid–solid coupling problem. Therefore, the proposed accurate and efficient method for predicting large-scale landslide water surges has become a major research area.

Numerical simulation is an important tool for landslide surge research to provide design optimization and reduce hazards (Zhang et al., 2022). In the past few decades, continuum-based and discontinuum-based methods are used to simulate the process of landslide surge (Quecedo et al., 2004; Cremonesi et al., 2011; Bosa and Petti, 2011; Abadie et al., 2010). Landslide and water are considered as two fluids to simulate the change in water surface after a landslide (Serrano et al., 2009), but the results hardly show the complex deformation in the interfacial flow. The study of landslide surge is generally a process of solid particles and fluid motion. Granular flow is suitable for landslide simulation due to the large deformation characteristics of landslides. Therefore, discrete element method (DEM) (Tang et al., 2009; Lo et al., 2011; Lin and Lin, 2015) is used to simulate the movement process and accumulation morphology of landslides along with the secondary hazards caused by landslides. And smooth particle hydrodynamics (SPH) is utilized to simulate liquid breaching and surge propagation (Monaghan,

* Corresponding authors at: College of Pipeline and Civil Engineering, China University of Petroleum (East China), Qingdao 266580, China.

** Corresponding authors at: College of Pipeline and Civil Engineering, China University of Petroleum (East China), Qingdao 266580, China

E-mail addresses: zhangyu@upc.edu.cn (Y. Zhang), s21060023@s.upc.edu.cn (S. Hou).

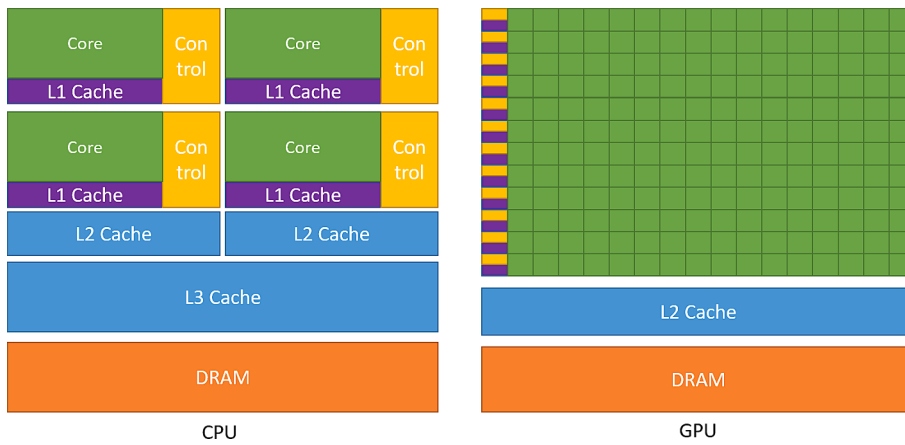


Fig. 1. The structure of CPU and GPU.

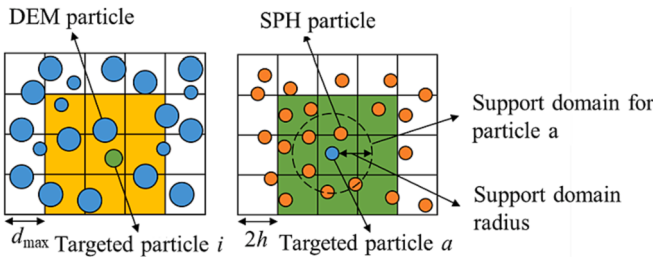


Fig. 2. Neighbor searching in the DEM and SPH modules.

2005), and a novel repulsive force particle boundary is proposed (Liang et al., 2023). The weakly compressible SPH method assumes that the fluid is weakly compressible (Zhang et al., 2022). The artificial equation of state is used to represent the weak compressibility of a liquid as an approximation to the incompressibility of a liquid in a real physical field. However, these studies have significant limitations on the effect of water on landslide movement. Fluid–solid interaction processes cannot be considered due to the neglect of energy transfer, including energy conversion from the landslide to water (Shan and Zhao, 2014) and the drag effect on the larger landslide front (Viroulet et al., 2014). DDA–SPH coupling method is proposed to conduct landslide surge simulation (Wang et al., 2016; Mikola, 2014), with the motions of the landslide and fluid solved by DDA and SPH, respectively. However, the coupling method is only applicable to the simulation of landslide surge by rigid slides due to the difficulty of DDA in simulating the large deformation behavior of granular slides.

In addition, DEM–SPH coupling have been proved to be effective in simulating complex interactions between fluid and solid (He et al., 2018; Sizkow and El Shamy, 2021). Therefore, DEM–SPH coupling is widely applicable to landslide surge simulations by rigid slides and granular slides. The interaction between the solid and fluid phases in the hybrid DEM–SPH model is simulated by drag and buoyancy forces. Tan and Chen (2017) used an incomplete solution of the DEM–SPH coupling method to simulate the 2D bulk landslide surge process, and the water slide surge simulation matched the experiment. A 3D nonhydrostatic model is used for the generation and propagation of waves to more accurately predict the hazards generated by landslide surges (Ma et al., 2015). Compared with those of 2D simulation, the computational volume of 3D simulation increases and the computational efficiency decreases, which becomes a difficult issue. The local averaging technique is proposed to improve the computational efficiency (Anderson and Jackson (1967)). The flow field in the local range around the DEM particles in this approach is interpolated by integrating the smooth kernel function to obtain the information. Then, the abovementioned

flow field information is transformed into the force on the DEM particles according to the coupled formulation. The Navier–Stokes equation based on local volume averaging is solved by SPH, and the reaction force of the DEM on the flow field is calculated by the local averaging method (Tsuij et al., 1993; Robinson et al., 2014). In addition, Graphics processing unit (GPU) parallel acceleration techniques are applied to DEM–SPH coupled computing. He et al. (2018) proposed a GPU-based DEM–SPH method to simulate particle flow with fluid level changes. GPU parallel computing uses multiple threads to execute a large number of relatively simple tasks in parallel to increase efficiency and the number of simulation particles (Zhang et al., 2023). However, landslide surge simulation with GPU parallel computing is rarely reported. High-performance framework structure and effective parallel acceleration technique provide accurate analysis of the physical processes of landslide particles.

In this study, we proposed a DEM–SPH coupling method with GPU parallel acceleration and local calculation technology, and developed the G-DeSp analysis software using C++ and Compute Unified Device Architecture (CUDA) languages to realize a 3D landslide surge simulation on the order of one million particles. Its accuracy and efficiency are verified by dam-break experiments. The influence of particle diameter on landslide surge is analyzed in the simulation of landslide surge, and the maximum climbing height of surge by bulk and rigid slide landslide bodies is compared and analyzed.

2. Coupled DEM–SPH calculation method

2.1. Governing equation of DEM and SPH

DEM–SPH is used for fluid–solid coupling simulation with DEM and SPH to simulate solids and fluids, respectively. For the ease of reading, the subscripts i and j denote DEM particles, and a and b denote SPH particles. According to Newton's second law, the motion equation of the solid particles is given by

$$m_i \frac{dv_i}{dt} = \sum_j F_{ij}^c + m_i g + f_i \quad (1)$$

$$I_i \frac{d\omega_i}{dt} = \sum_j T_{ij} \quad (2)$$

where m_i and v_i are the mass and velocity of particle i , respectively; F_{ij}^c is the contact force on particle i due to particle j , g is gravitational acceleration, I_i is moment of inertia, ω_i is the angular velocity, and T_{ij} is the contact torque on particle i due to particle j .

For a fluid, the continuum is discretized into mutually independent particles with properties such as fluid position, velocity, density, pressure, and interaction forces. The fluid continuity equation in SPH is

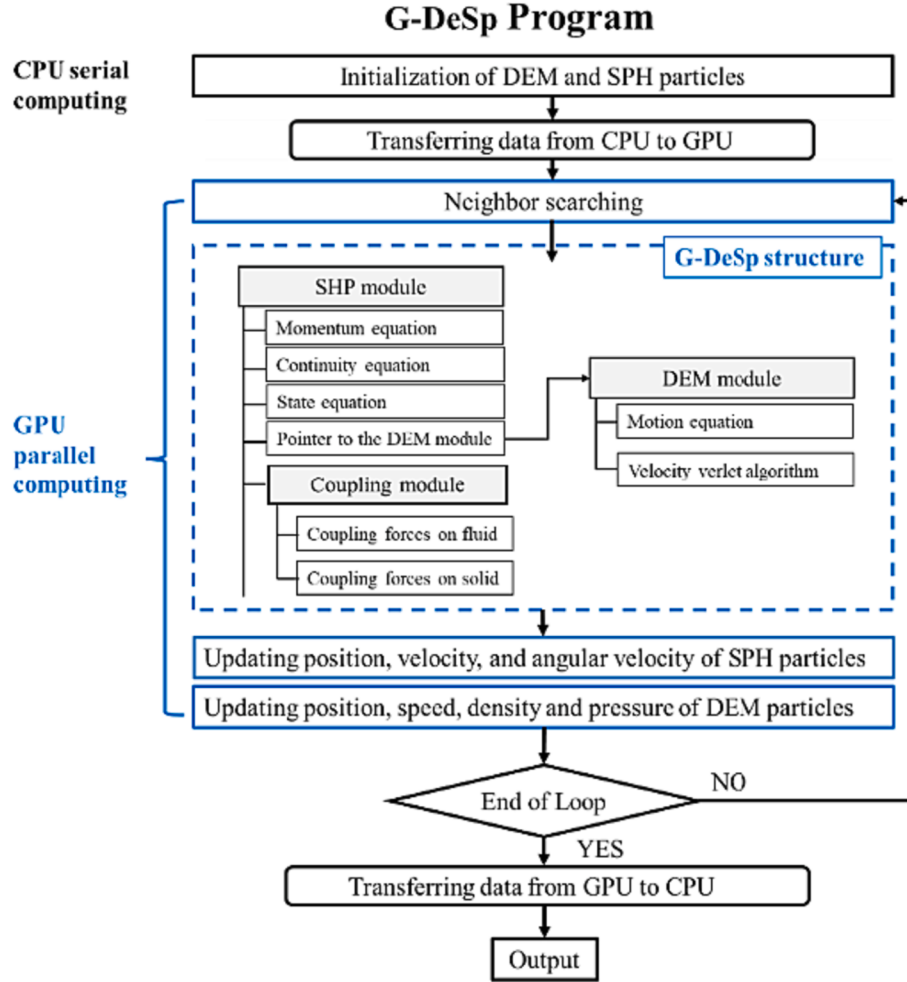


Fig. 3. Flowchart of GPU-based calculation in the proposed method.

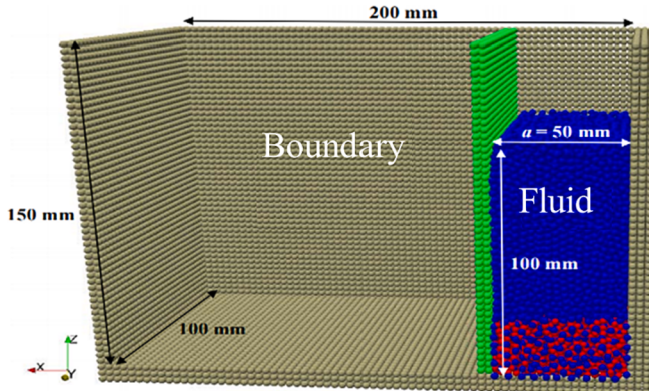


Fig. 4. Configuration of the two-phase dam-break simulation.

given by

$$\frac{D\bar{\rho}_a}{Dt} = \sum_b m_b v_{ab} \nabla_a W_{ab}(h) \quad (3)$$

where $\bar{\rho}_a$ is the local average density of particle a , $v_{ab} = v_a - v_b$, v_a and v_b are the velocities of particle a and b , respectively; $W_{ab}(h)$ is the simplified form of the kernel function $W(|r_a - r_b|, h)$, and Wendland's kernel function (Wendland, 1995) is adopted

Table 1
Parameters in the two-phase dam-break simulation.

Parameter	Symbol	Value	Unit
Initial spacing SPH particle	Δp	3.0	mm
Smooth length	h	$1.3\Delta p$	mm
Time step	Δt_f	5.0×10^{-6}	s
Stiffness	—	1000	N/m
Recovery coefficient	—	0.9	—
Friction coefficient	μ	0.2	—

$$W(|r_a - r_b|, h_a) = \alpha_D \begin{cases} \left(1 - \frac{q}{2}\right)^4 (1 + 2q) & 0 \leq q \leq 2 \\ 0 & q > 2 \end{cases} \quad (4)$$

where $\alpha_D = 7/(8\pi h^3)$ in three dimensions and $q = |r_a - r_b|/h$, r_a and r_b are the positions of particles a and b , respectively; h is the smoothing length of the SPH particle, $h = \sigma \Delta p$, σ is the interpolation resolution normally set to 1.3 (Monaghan, 2005) and Δp is the initial spacing.

The momentum equation of fluid in SPH is given by (Morris et al. 1997)

$$\frac{Dv_a}{Dt} = - \sum_b m_b \left(\frac{P_a}{\bar{\rho}_a} + \frac{P_b}{\bar{\rho}_b} \right) \nabla_a W_{ab}(h) + \Pi_{ab} + g + \frac{f_a}{m_a} \quad (5)$$

$$\Pi_{ab} = \sum_b m_b \frac{2\mu_f r_{ab} \cdot \nabla_a W_{ab}(h)}{\rho_a \rho_b (r_{ab}^2 + 0.01h^2)} v_{ab} \quad (6)$$

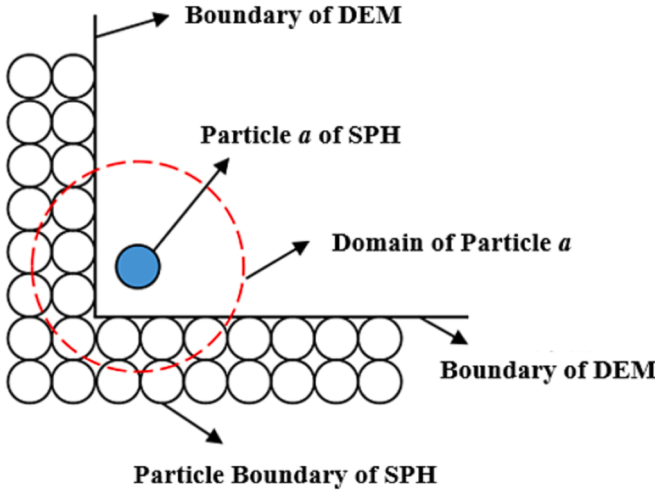


Fig. 5. DEM and SPH boundaries.

where P_a and P_b are the pressures of particles a and b , respectively; f_a is the coupling force on particle a due to neighboring DEM particles, $r_{ab} = r_a - r_b$, r_a and r_b are location of particle a and b , respectively; μ_f is the dynamic viscosity of the fluid.

The weakly compressible SPH method with controlled density is used and the artificial state equation is given by

$$P_a = B \left(\left(\frac{\bar{\rho}_a}{\varepsilon_a \rho_0} \right)^{\gamma} - 1 \right) \quad (7)$$

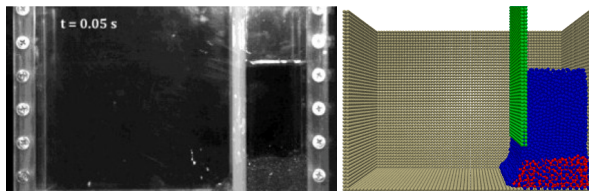
$$B = \frac{\rho_0 c^2}{\gamma} \quad (8)$$

2.2. DEM-SPH coupling

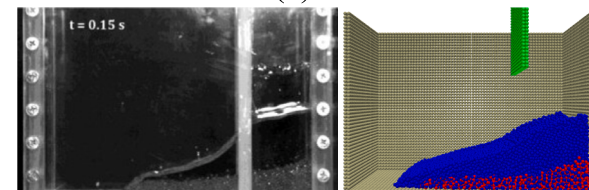
During the coupling process, the fluid-solid coupling force between the solid and the fluid is solved by buoyancy and drag force. The fluid-solid coupling force on the DEM particles is

$$f_i = f_i^{buoyancy} + f_i^{drag} \quad (9)$$

where $f_i^{buoyancy}$ and f_i^{drag} are the buoyancy and drag force on particle i due to neighboring SPH particles, respectively. $f_i^{buoyancy}$ and f_i^{drag} are expressed as (Sun et al. 2013)



(a) $t=0.05$ s



(c) $t=0.15$ s

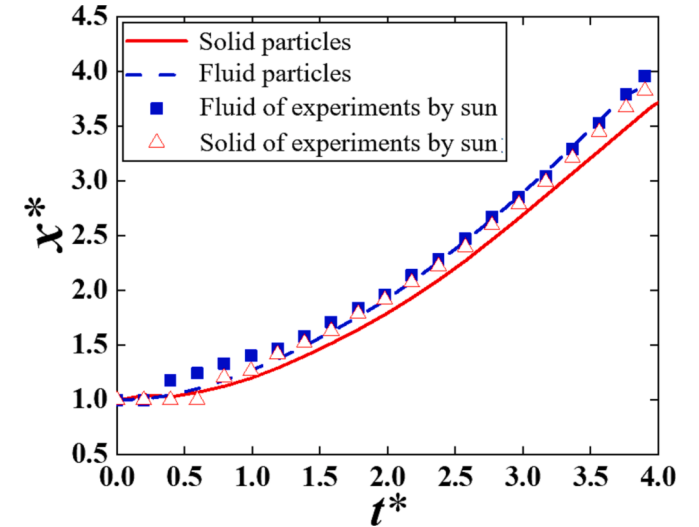


Fig. 7. Propagation profiles of waves and solid particles in the experiment (Sun et al., 2013) and DEM-SPH simulation.

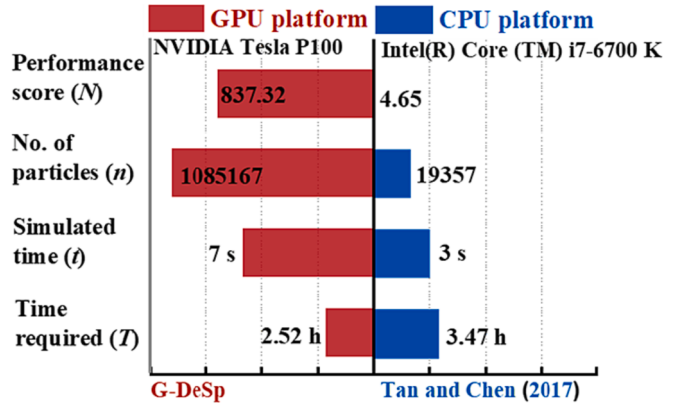
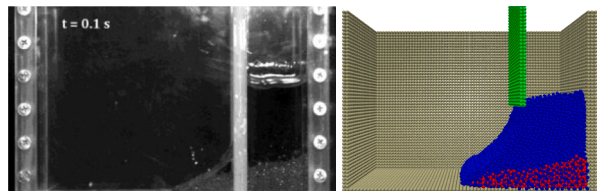
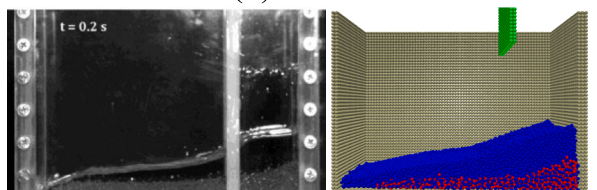


Fig. 8. The comparison of the performance between G-DeSp and another program base on CPU.



(b) $t=0.1$ s



(d) $t=0.2$ s

Fig. 6. Comparison of the experimental results (left) and G-DeSp (right) of two-phase dam-break.

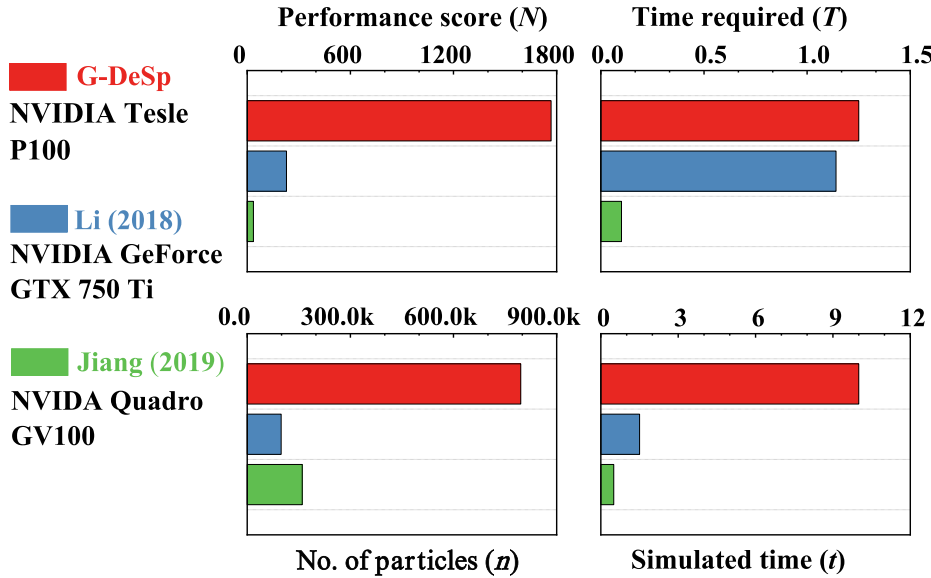


Fig. 9. The comparison of the performance between G-DeSp and other programs base on GPU.

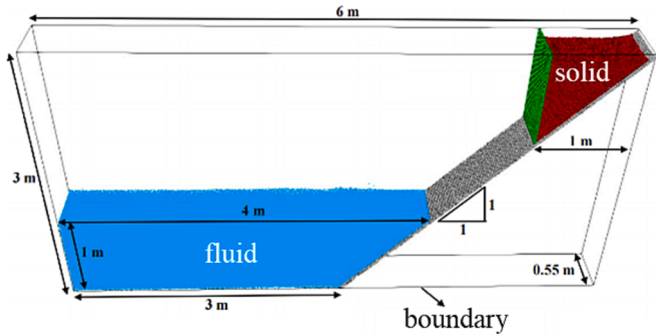


Fig. 10. Configuration of the simulation of landslide surge by granular slide.

Table 2

Simulation parameters of landslide surge by granular slide (Tan and Chen, 2017).

Parameters	Symbols	value	unit
Initial spacing SPH particles	Δp	18.18	mm
Smooth length	h	$1.3\Delta p$	mm
Time step	Δt_f	5.0×10^{-6}	s
Elastic modulus of DEM particles	E	2×10^8	Pa
Poisson's ratio of DEM particles	ν	0.3	—
Friction coefficient	μ	0.364	—

$$\mathbf{f}_i^{buoyancy} = -V_i \sum_a \frac{m_a P_a}{\rho_a} \nabla_i W_{ia}(h_c) \quad (10)$$

$$\mathbf{f}_i^{drag} = \frac{\beta_i V_i}{1 - \varepsilon_i} (\mathbf{u}_i - \mathbf{v}_i) \quad (11)$$

where β_i is the interphase momentum exchange coefficient and V_i is the volume of particle i , ε_i and \mathbf{u}_i are the local porosity of particle i and fluid velocity at the position of particle i , respectively.

$$\varepsilon_i = \sum_a \frac{m_a}{\rho_a} W_{ia}(h_c) / \sum_a \frac{m_a}{\rho_a} W_{ia}(h_c) \quad (12)$$

$$\mathbf{u}_i = \frac{1}{\sum_a \frac{m_a}{\rho_a} W_{ia}(h_c)} \sum_a \frac{m_a}{\rho_a} \mathbf{W}_{ia}(h_c) \quad (13)$$

The interphase momentum exchange coefficient β_i is expressed as

$$\beta_i = \begin{cases} 150 \frac{(1 - \varepsilon_i)^2}{\varepsilon_i} \frac{\rho_f}{d_i^2} + 1.75(1 - \varepsilon_i) \frac{\rho_f}{d_i} |\mathbf{u}_i - \mathbf{v}_i|, & \varepsilon_i \leq 0.8 \\ 0.75 C_d \frac{\varepsilon_i(1 - \varepsilon_i)}{d_i} \rho_f |\mathbf{u}_i - \mathbf{v}_i| \varepsilon_i^{-2.65}, & \varepsilon_i > 0.8 \end{cases} \quad (14)$$

where d_i , ρ_f , and C_d are the diameter of particle i , density of the fluid and drag coefficient, respectively. The drag coefficient C_d is given by

$$C_d = \begin{cases} \frac{24}{Re_i} (1 + 0.15 Re_i^{0.687}) & Re_i \leq 1000 \\ 0.44 & Re_i > 1000 \end{cases} \quad (15)$$

where Re_i is the Reynolds number of particle i :

$$Re_i = \frac{\rho_f d_i \varepsilon_i |\mathbf{u}_i - \mathbf{v}_i|}{\mu_f} \quad (16)$$

According to Robinson et al. (2014), the fluid–solid coupling force on particle a is relevant to its mass and density and the coupling forces on the neighboring DEM particles, and it is expressed as

$$\mathbf{f}_a = -\frac{m_a}{\rho_a} \sum_i \frac{1}{S_i} \mathbf{f}_i W_{ai}(h_c) \quad (17)$$

$$S_i = \sum_a \frac{m_a}{\rho_a} W_{ia}(h_c) \quad (18)$$

where \mathbf{f}_i is the coupling force on particle i .

3. the DEM–SPH coupling program: G-DeSp

3.1. G-DeSp implementation

G-DeSp is a DEM–SPH coupling program with full intellectual property rights based on GPU platform parallel acceleration technique. The internal structure of a CPU and a GPU is shown in Fig. 1, where the number of cores inside a GPU is much larger than that of a CPU. More controllers and cache memories give CPU an advantage in handling complex logic operations, while the structural design of GPU has a lot of operators, which makes GPU faster in handling a large number of simple and repetitive numerical operations. GPU have more computational cores than CPU, allowing for greater data throughput for shorter periods

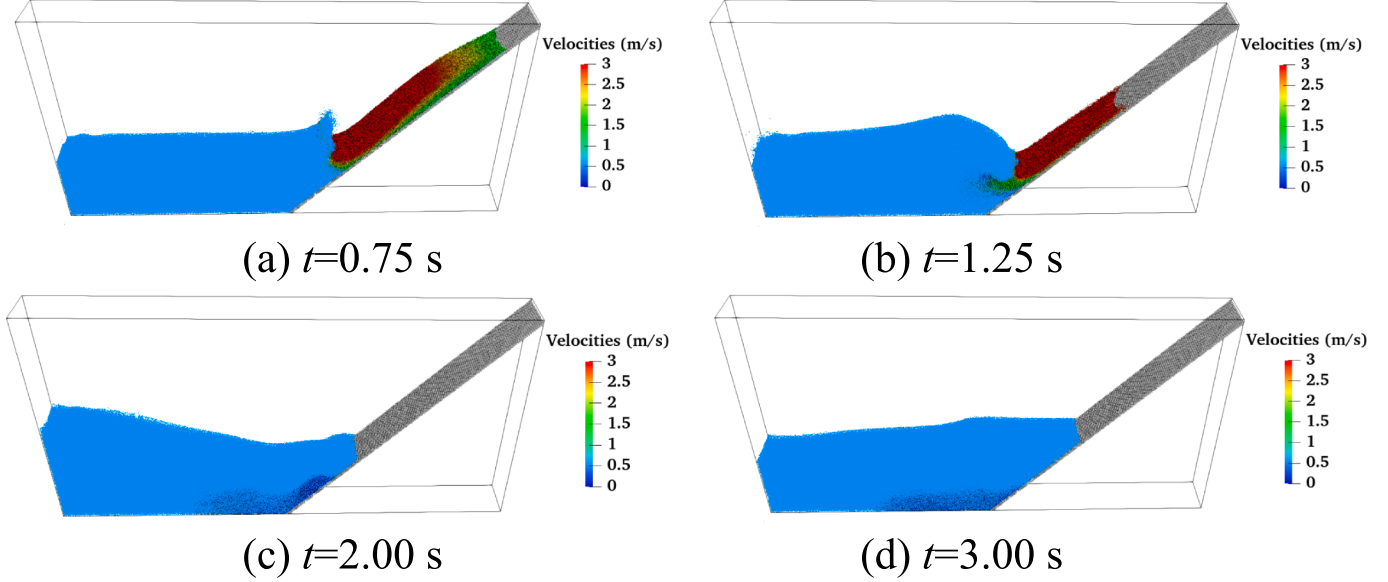


Fig. 11. Process of landslide surge by granular slide.

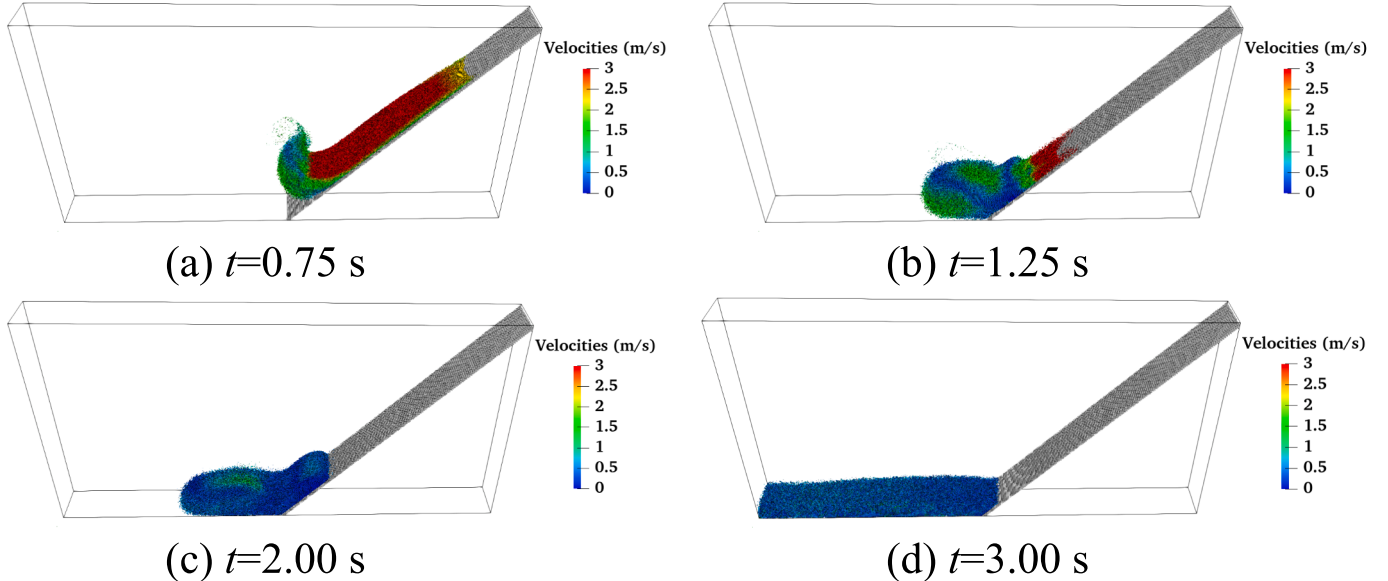


Fig. 12. The state of solid particles in landslide surge.

of time. And GPU are based on shared memory, which reduces the time required for thread switching in parallel computing. In CUDA, the GPU is divided into multiple grids containing blocks whose internal data can be shared. A block is subdivided into many threads, the smallest unit of computation, which are physically mapped to the GPU core. A thread is responsible for the computation of only one data unit. This special architecture allows GPU processing to execute a computational task in parallel on multiple threads. The threads are independent of each other and do not affect each other.

Neighbor searching is the most time-consuming process in the algorithm, which directly affects the computational speed and efficiency. The searching method consists of particle mapping and searching. The computational domain is divided into a number of regular cubes meshes. In DEM module, the grid needs to accommodate the largest DEM particle, and the grid length the diameter of the largest DEM particle, d_{\max} . In SPH module, the grid where the targeted SPH particle is located and its neighboring grids form a large grid that needs to accommodate the

support domain of the target SPH particle, and the grid length is twice the smooth length, $2h$ (Fig. 2). A dual-grid searching method is proposed to reduce the size of the support domain and accelerate the neighbor searching. First, the DEM particles are mapped to a grid to search for DEM particles, and the hash value of each grid is calculated based on the location. Then indexing relationships are created and the position of these particles are calculated, which can contact with other particles located in the support domain of the target particles. Finally, the SPH particles are mapped to the grid and the same operation is performed.

Therefore, finding and calculating particles in contact with the target particles is not to check all particles, but only the particles located and in the adjacent grid. The number of particles that need to be checked is greatly reduced, so the speed and efficiency of the neighborhood search is greatly improved. In addition, the method can avoid the atomic operations in GPU programming, and maximize performance.

The main part of G-DeSp consists of the DEM, SPH and the coupling modules. The SPH module is the core of the program and contains an

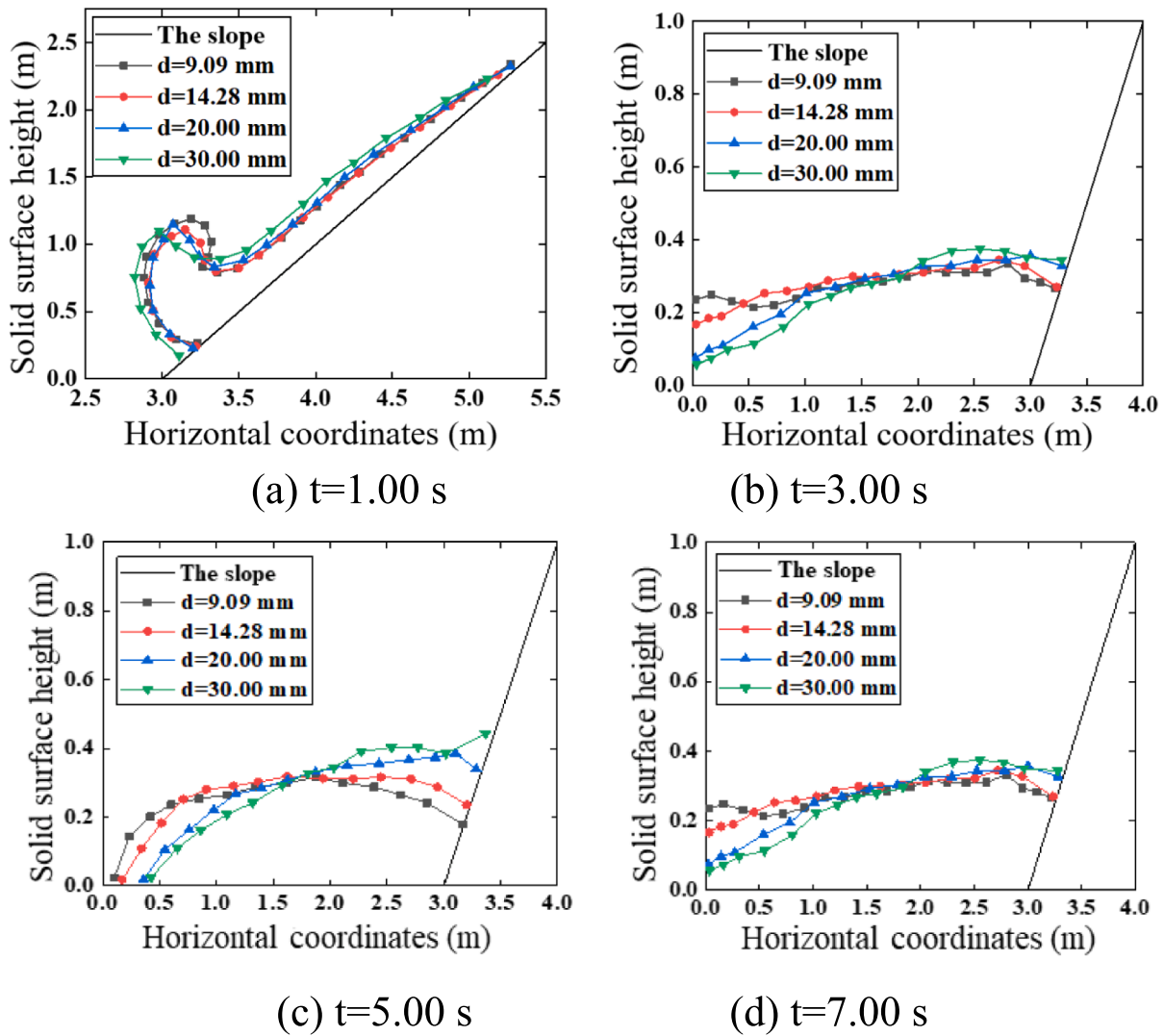


Fig. 13. Comparison of the surface profiles of granular slides with different diameters of solid particles.

internal pointer to the DEM module, which allows us to call the member functions of the DEM module and access the array of this module from within the SPH module. Meanwhile, the coupled module is inserted inside the SPH module. All functions of the coupling module are set as members of the SPH module (Fig. 3). Thus, all operation on SPH particles or DEM particles can be performed inside the SPH module. A member function “*OneTimeStep*” defined inside the SPH module, which contains all the operations that need to be performed in one time step. A member function “*Run*” is defined, which is a function that calls the function “*OneTimeStep*” continuously through a loop, and the condition for jumping out of the loop is that the computation time is greater than the set simulation time.

The preprocessing module (particle data initialization) and the postprocessing module (data output) are executed serially on the CPU platform. The computational process is built based on the GPU parallel acceleration algorithm, and the neighbor searching, force calculation, and property update of all particles in the simulation are computed in parallel and synchronously on the GPU platform. This way fully utilizes the advantages of parallel acceleration of the GPU platform, which greatly enhances the computational efficiency.

3.2. Program verification

A typical two-phase dam-break simulation is used to verify the

accuracy of G-DeSp. The simulation configuration is shown in Fig. 4 according to the experiment of Sun et al. (2013) where blue, red, green, and brown particles are fluid particles, solid particles, moving gate, and wall boundary, respectively. The smooth length of the SPH particles has to be greater than twice the diameter of the discrete element particles in order to make the local porosity spatially continuous, and the simulation parameters are shown in Table 1. Initializing the fluid and solid particles, the gate is lifted upward at a speed of 0.68 m/s, and the moment is $t = 0$ s.

The wall is a dynamic particle boundary for SPH particles, and multiple layers of boundary particles are arranged immediately outside of the boundary with exactly the same properties as the internal fluid particles. A mesh boundary is used for DEM particles, which is consistent with the simplified Hertz-Mindlin contact model (Fig. 5).

A comparison of Sun et al. (2013) and G-DeSp is shown in Fig. 6. The simulation agrees well with the experiment. The program accurately reproduces the fluid flow, the motion of solid particles, the interaction between fluid and solid particles, and the limiting effect of boundaries and gates on fluid and solid particles.

For quantitative comparison, two dimensionless numbers are defined to describe the propagations of the wave and solid particle front, and they are expressed as

$$t^* = t(2|g|/H)^{0.5} \quad (19)$$

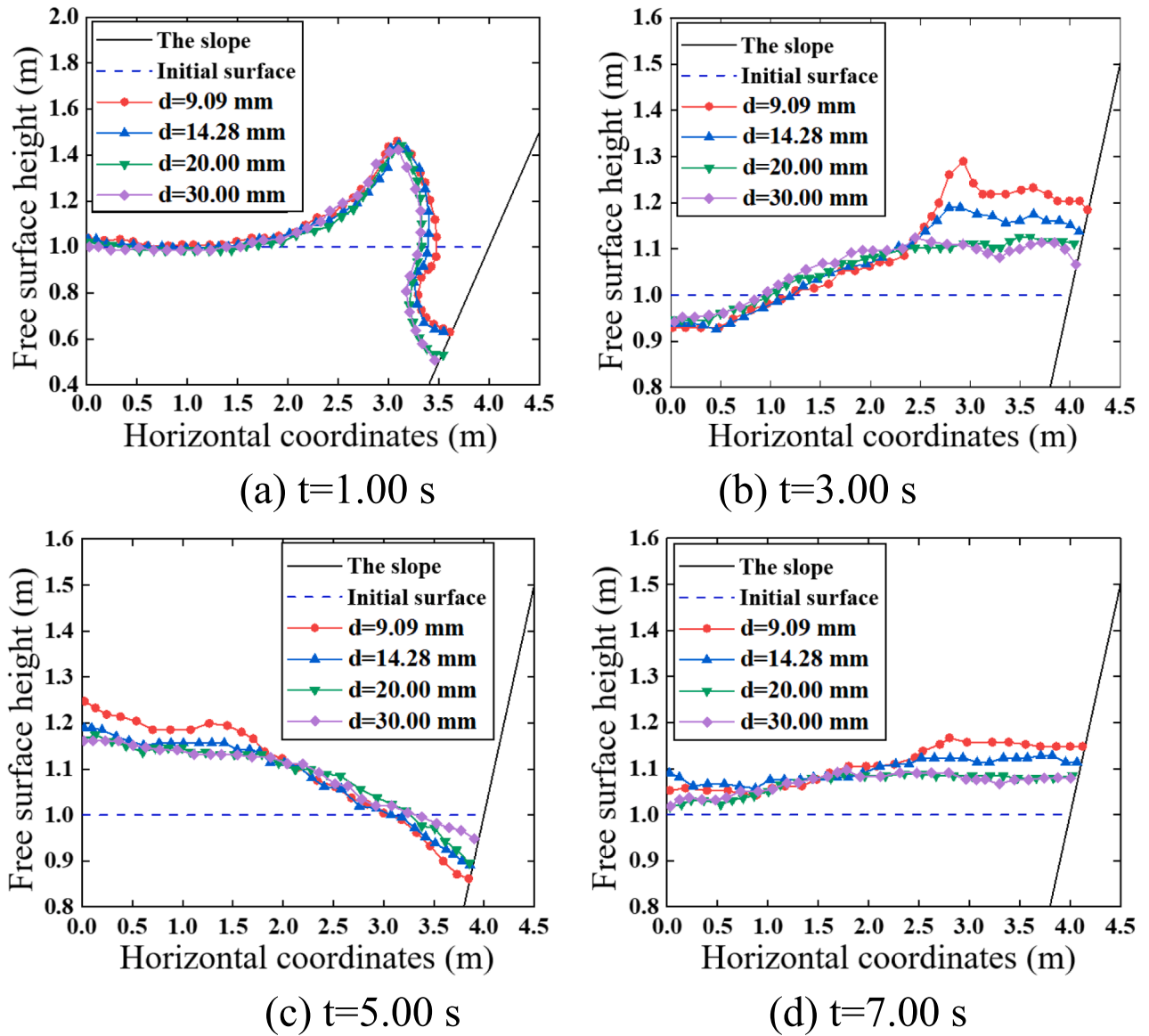


Fig. 14. Comparison of surge slides with different diameters of solid particles.

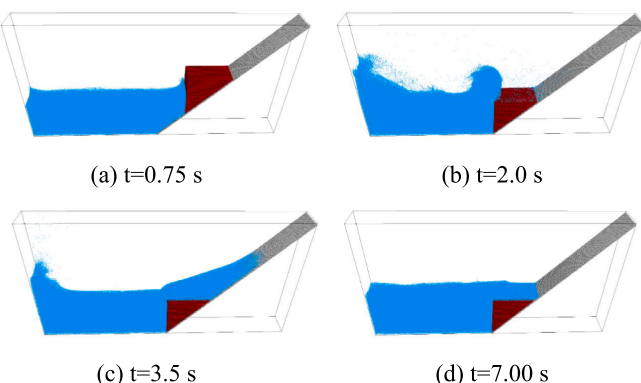


Fig. 15. The process of landslide surge caused by rigid slide in DEM-SPH simulation.

$$x^* = x/H$$

(20)

where t and x are the calculation time starting from the instant of lifting the gate and position of wave or solid particle front, respectively. $|g|$ is the magnitude of the acceleration of gravity, equal to 9.8; H is initial length of the fluid.

The variation in the position of the left end of the fluid and solid particle accumulation with time is shown in Fig. 7. The experimental and simulated results are matched, and the velocity of the wave front is observed to be slightly higher than that of the solid particle front in both.

To quantitatively describe the computational performance of the numerical simulation program, the performance score is defined:

$$N = \frac{n \cdot t}{T} \quad (21)$$

where N is performance score, the larger N is, the more computationally powerful the program is; n is the number of particles simulated, t is simulated time, T is time required.

Compared to the CPU program (Tan and Chen, 2017), less time is required when both the number of particles and the simulation time are higher than the CPU program in the case of landslide surge (Fig. 8). The

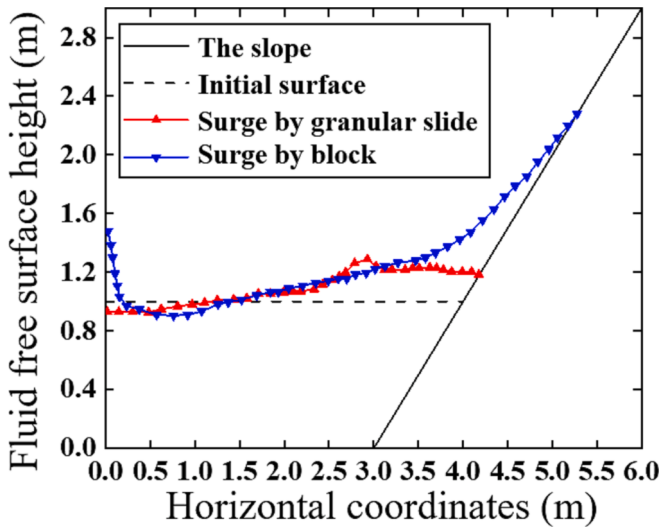


Fig. 16. Comparison of the clime height of surge by granular slide and rigid slide.

overall performance score is much higher than the CPU program. Compared to the GPU program (Jiang, 2019; Li, 2021), under conditions with a higher number of particles and a longer simulation time, the performance score is still the highest, even though it takes more time in the case of single-phase flow dam failure (Fig. 9).

4. Landslide surge

4.1. Landslide surge by granular slide

The simulation configuration of landslide surge is shown in Fig. 10, where blue, red, green and white particles denote the fluid, granular slide, movable gate, and slope surface, respectively. The numbers of DEM and SPH particles are 386,468 and 698,699, respectively, with a simulation time of 7 s and a calculation time of 2.52 h. The boundary conditions are consistent with the dam-break simulation. The SPH boundary particles are not shown in the figure below for the sake of clear presentation of the results. All relevant parameters are listed in Table 2.

The results of the landslide surge by the granular slide are shown in Fig. 11, where the color of the solid particles is its velocity and the blue particles are fluid. At the beginning of the landslide, the granular slide along the slope under the effect of gravity, in which the velocity of solid particles at the critical surface is the largest, gradually decreases to the right. With the solid particles into the water, the fluid absorbs partial kinetic energy of the landslide transformed into its own kinetic and potential energy, which causes the surge to be generated on the right

and propagate to the left. At $t = 2.00$ s, the landslide body has been fully immersed in the water. At this time, the left side of the fluid surface rises significantly due to the wave propagation of the surge to the left side of the boundary. Then the surge propagates to the right until it completely dissipates and the free fluid surface returns to calm. The fluid surface is significantly higher than the initial hydrostatic surface due to the large volume of the landslide submerged in the fluid.

Solid particles are plotted separately to show the location and morphology of solid particles during landslide surges due to obscuration by fluid particles (Fig. 12). The leading edge of the solid particles is supported by the fluid after entering the water, and an obvious “buckling” phenomenon appears. The solid particles are hindered by the water body, the leading-edge velocity is reduced, and solid particles at the leading edge are agglomerated, which forms a spherical shape. Under the dragging force of fluid, the landslide accumulation gradually moves to the left side and finally flattens out and stably accumulates at the bottom.

4.2. Influence of the diameter of solid particles on the landslide surge

Four sizes of solid particles $d = 9.09\text{mm}$, $d = 14.28\text{ mm}$, $d = 20.00\text{ mm}$ and $d = 30.00\text{ mm}$ are selected to conduct the landslide surge simulation with the same simulation parameters as the abovementioned landslide surge simulation.

The morphology and displacement of solid particles are consistent for different particle diameters in the initial stage (Fig. 13). However, after 3.00 s, the volume of the leading edge of the landslide decreases with the increase in the diameter of solid particles, and the volume of the trailing part of the landslide rises with the increment in the diameter of solid particles. Subsequently, a large number of solid particles move from the slope to the bottom of the flume, and the displacement of the leading edge and trailing part of the landslide decreases with the increase in the diameter of solid particles. Therefore, the diameter of solid particles significantly influences their movement and morphology. The velocity and displacement of solid particles decrease as the diameter increases, and the form of “small volume at the leading edge and large volume at the trailing part” is more obvious when the diameter is larger.

The landslide surge pattern is consistent in the initial stage of

Table A1
Parameters in the 2D DEM simulation of soil collapse.

Parameters	Symbols	value	unit
Particle diameter	d	$1.0 \sim 1.5$	mm
Density	ρ_s	1800	kg/m^3
Elastic modulus	E	8.4×10^5	Pa
Poisson's ratio	ν	0.3	—
Frictional coefficient	μ	0.36	—
Time step	Δt_s	1.0×10^{-5}	s

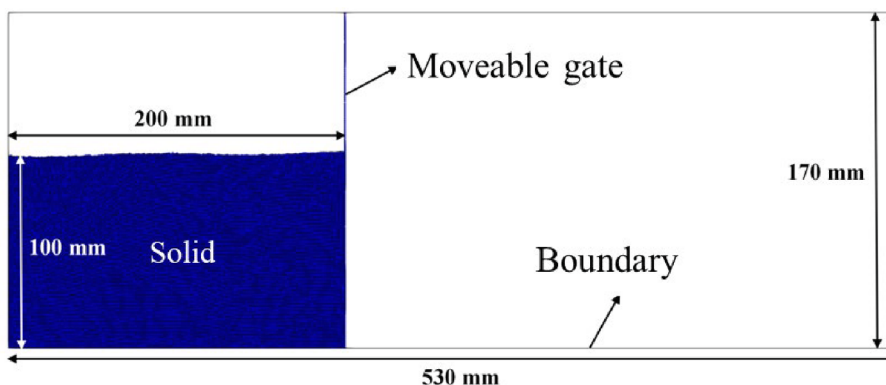


Fig. A1. Configuration of the 2D DEM simulation of soil collapse.

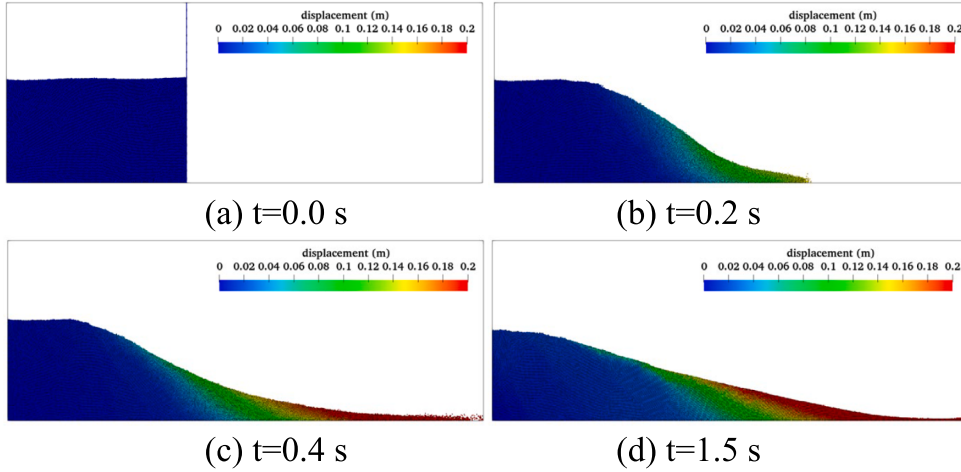


Fig. A3. Evolution of the soil displacement and surface profiles during the collapse process in DEM simulation.

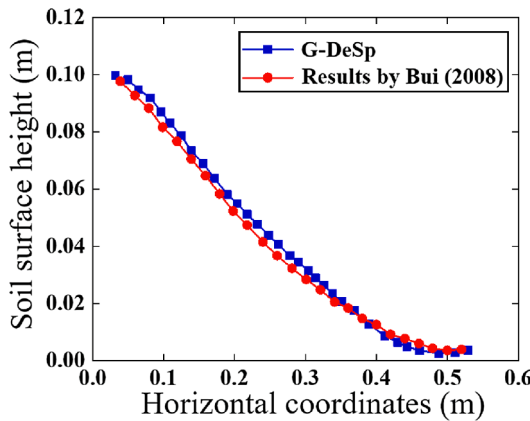


Fig. A4. Comparison of the surface profiles of soil after collapse processes in the experiment (Bui et al. 2008) and DEM simulation.

different particle diameters (Fig. 14). However, after 3.00 s, the surge is located on the right side of the fluid, and the surge height and climb height first increase with the rise in solid particle diameter and then decrease. Subsequently, the surge propagates to the left side of the water body, and the surge height still first rises with the increase in solid particle diameter and then decreases. The free fluid surface height first rises with the increase in solid particle diameter and then decreases under different particle diameters when the surge has been dissipated. Therefore, the influence of the diameter of solid particles on surge is significant by landslide, and surge intensity strengthens with increasing

solid particle diameter at the slope and weakens at a distance.

4.3. Landslide surge by rigid slide

The landslide body is changed from a bulk to a rigid slide of the same volume, and the simulation parameters are consistent with Table 2 in conducting landslide surge by rigid slide.

After contact with the rigid landslide, the water propagates to the left and tends to move upward at the contact surface with the landslide (Fig. 15). The fluid scattered to the left collides with the left border and climbs significantly higher. Given that the water is restricted by the left boundary and gravity, it starts to flow back to the right and spreads over the top of the landslide to continue upward along the slope, which climbs to a higher position. The fluid-free surface then began to stabilize, which completely submerges the landslide body in the water column. Considering that the landslide body drains a large amount of water, the free fluid level of the water is remarkably higher than the initial hydrostatic surface at this time.

Compared with the bulk landslide body, the rigid slide leads to a more violent surge (Fig. 16). The maximum climbing height of surge by the rigid slide are as 6.5 times as those of surge by the granular slide with

Table A2
Parameters in the single-phase dam-break simulation.

Parameters	Symbols	Value	Unit
Initial spacing of SPH particles	Δp	$H/30$	mm
Smoothing length	h	$1.3\Delta p$	mm
Time-step	Δt_f	1.0×10^{-5}	s

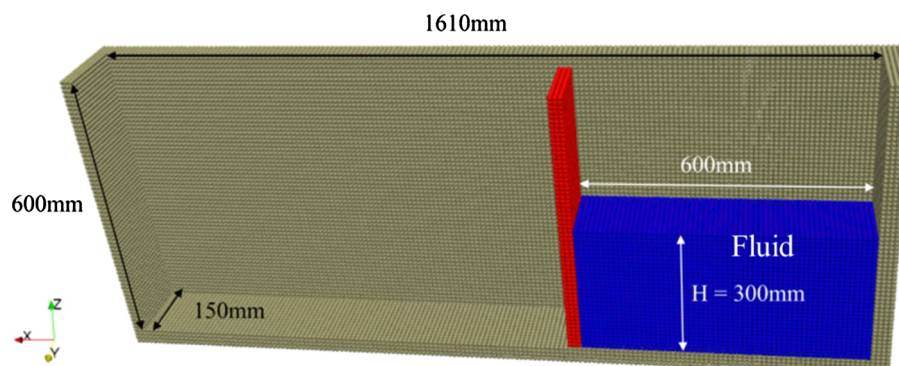


Fig. A5. The configuration of the single-phase dam-break simulation.

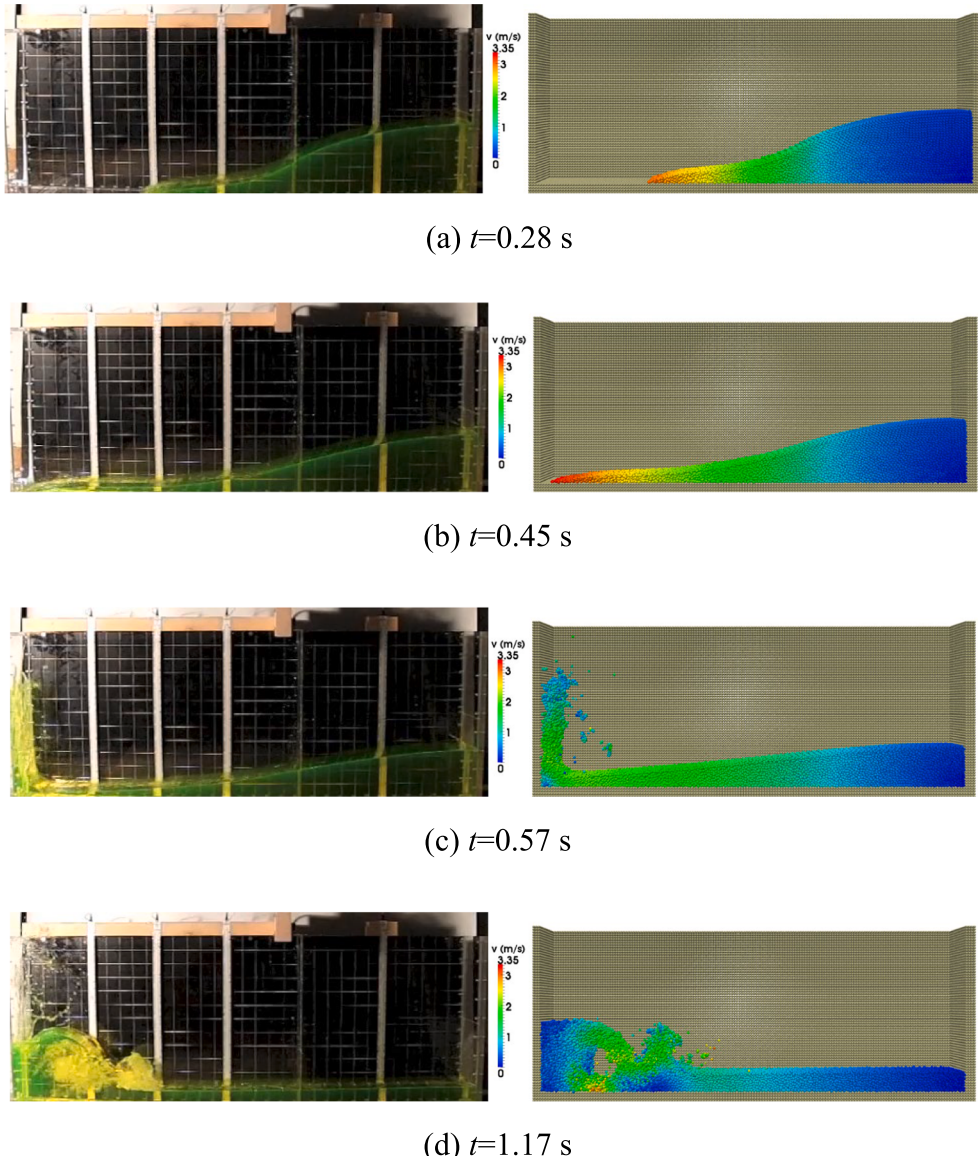


Fig. A6. Single-phase dam-break: free surface profiles in the experiment (Lobovský et al. 2014) (left) and SPH simulation (right).

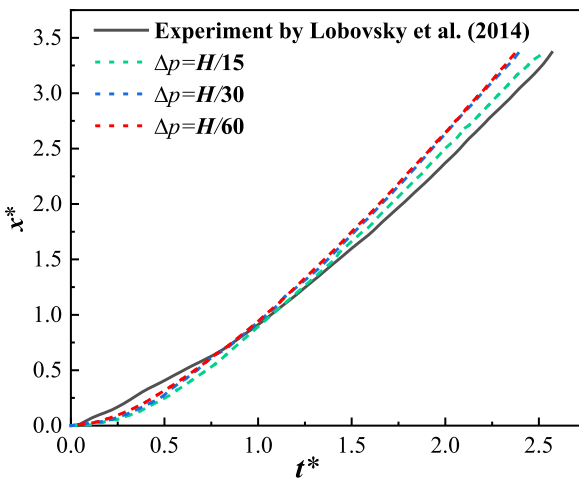


Fig. A7. Single-phase dam-break: propagation of the wave front in the experiment (Lobovský et al., 2014) and SPH simulation.

the same volume, indicating that the surge hazard induced by rigid slide is much more serious than that induced by granular slide. Solid particles collide with the water one after another, which results in the water being subject to a smaller fluid–solid coupling force. The energy of the bulk particles is dissipated in the sliding process inside the landslide body, and the energy transferred from the landslide body to the water body is reduced. However, the rigid slide does not deform in the sliding process, and no loss of kinetic energy transfer from the landslide body to the water occurs. A large number of solid particles interact with the water at the same moment, and the water is subject to a larger fluid–solid coupling force.

5. Conclusions

In this study, we proposed a DEM–SPH coupling method with GPU parallel acceleration and local calculation technology, developed G-DeSp program to realize a 3D landslide surge simulation by granular slide and rigid slide on the order of one million particles. The main conclusions are as follows:

- (1). G-DeSp adopts the neighbor search method and executes all the computation modules on the GPU platform, taking full advantage of its parallel accelerated computation, which improved the computation efficiency.
- (2). The leading edge of the solid particles is supported by the fluid after entering the water, and an obvious “buckling” phenomenon appears in landslide surge by granular slide. The solid particles are hindered by the water body, the leading-edge velocity is reduced, and solid particles at the leading edge are agglomerated, which forms a spherical shape. Under the dragging force of fluid, the landslide accumulation gradually moves to the left side and finally flattens out and stably accumulates at the bottom.
- (3). The influence of the diameter of solid particles on surge is significant by landslide, and surge intensity strengthens with increasing solid particle diameter at the slope and weakens at a distance. The maximum climbing height of surge by the rigid slide are as 6.5 times as those of surge by the granular slide with the same volume, indicating that the surge hazard induced by rigid slide is much more serious than that induced by granular slide.

Future work on secondary surge hazards will be conducted to further improve computational modeling capabilities.

Appendix. . Independent validation of DEM model and SPH model

1. Validation of DEM model

The independent DEM model is validated by experiment of two-dimensional soil collapse conducted by [Bui et al. \(2008\)](#) ([Fig. A1.](#)), and the relevant DEM parameters are listed in [Table A1.](#). The blue particles are DEM particles, the vertical line is the moveable gate, and the black border is the DEM boundary.

The displacement of soil particles and the change of soil morphology in the two-dimensional soil collapse simulation are shown in [Fig. A3.](#), where the color of soil particles indicates the displacement of soil particles. After the gate is removed, the soil collapses under the action of gravity, and the displacement of soil particles at the top of the soil body is the largest, and the soil body in the lower left region is the least disturbed. The computed free surface profiles of fluid and distribution of solid particles are in good agreement with experimental results generally ([Fig. A4.](#)).

2. Validation of SPH model

The independent SPH model is validated by test of single-phase dam-break conducted by [Lobovský et al. \(2014\)](#) ([Fig. A5.](#)), where brown, red and blue particles represent the wall boundaries, moveable gate and fluid, respectively. The relevant SPH parameters are listed in [Table A2](#). The Velocity Verlet algorithm is used to update the density, velocity, and position of SPH particles:

$$\rho_a^{n+1} = \rho_a^n + \frac{1}{2} \left[\left(\frac{D\rho_a}{Dt} \right)^n + \left(\frac{D\rho_a}{Dt} \right)^{n+1} \right] \Delta t \quad (\text{A.1})$$

$$\mathbf{v}_a^{n+1} = \mathbf{v}_a^n + \frac{1}{2} \left[\left(\frac{D\mathbf{v}_a}{Dt} \right)^n + \left(\frac{D\mathbf{v}_a}{Dt} \right)^{n+1} \right] \Delta t \quad (\text{A.2})$$

$$\mathbf{r}_a^{n+1} = \mathbf{r}_a^n + \mathbf{v}_a^n \Delta t + \frac{1}{2} \left(\frac{D\mathbf{v}_a}{Dt} \right)^n \Delta t^2 \quad (\text{A.3})$$

where ρ_a^n , $\left(\frac{D\rho_a}{Dt} \right)^n$, \mathbf{r}_a^n , \mathbf{v}_a^n , $\left(\frac{D\mathbf{v}_a}{Dt} \right)^n$, ρ_a^{n+1} , $\left(\frac{D\rho_a}{Dt} \right)^{n+1}$, \mathbf{r}_a^{n+1} , \mathbf{v}_a^{n+1} and $\left(\frac{D\mathbf{v}_a}{Dt} \right)^{n+1}$ is the density, density change rate, position, velocity and acceleration of particle a at step n and n + 1, respectively; Δt is time step.

The computed free surface profiles are compared with experiment ([Fig. A6.](#)). The propagation of wave front and confining of vertical wall on water flow are well reproduced. And the effect of initial spacing of SPH particles on the behavior of water flow is shown in [Fig. A7..](#) The computed propagation velocity of the wave front increases slightly and tends to more disagree with the experimental result with the decease of initial spacing of SPH particles, indicating that numerical accuracy of the proposed model can be improved by choosing an appropriate initial spacing of SPH particles.

References

Abadie, S., Morichon, D., Grilli, S., et al., 2010. Numerical simulation of waves generated by landslides using a multiple-fluid Navier-Stokes model. *Coast. Eng.* 57 (9), 779–794.

CRediT authorship contribution statement

Yu Zhang: Methodology, Resources, Supervision. **Shaohao Hou:** Methodology, Investigation, Formal analysis, Writing – original draft. **Shengjie Di:** Writing – review & editing. **Zaobao Liu:** Writing – review & editing. **Yifan Xu:** Writing – review & editing.

Declaration of Competing Interest

The authors declare that they have no known competing financial interests or personal relationships that could have appeared to influence the work reported in this paper.

Data availability

No data was used for the research described in the article.

Acknowledgements

This work was supported by China Natural Science Foundation (No. 51890914; No. 52179119); and Natural Science Foundation of Shandong Province (No. ZR2019MEE001). The authors gratefully acknowledge the valuable comments and suggestions from reviewers.

- Bui, H., Fukagawa, R., Sako, K., et al., 2008. Lagrangian meshfree particles method (SPH) for large deformation and failure flows of geomaterial using elastic-plastic soil constitutive model. *Int. J. Numer. Anal. Methods. Geomech.* 32 (12), 1537–1570.
- Cremonesi, M., Frangi, A., Perego, U., 2011. A Lagrangian finite element approach for the simulation of water-waves induced by landslides. *Comput. Struct.* 89 (11), 1086–1093.
- Fritz, H., Hager, W., Minor, H., 2001. Lituya bay case: Rockslide impact and wave run-up. *Sci. Tsunami Hazards.* 19, 22.
- Fritz, H., Hager, W., Minor, H., 2003. Landslide generated impulse waves, Part 2: Hydrodynamic impact craters. *Exp. Fluids* 35 (6), 520–532.
- He, Y., Andrew, E., Bayly, A.H., 2018. A GPU-based coupled SPH-DEM method for particle-fluid flow with free surfaces. *Powder Technol.* 338, 548–562.
- V. Heller, 2007. Landslide Generated Impulse Waves: Prediction of Near Field Characteristics. ETH Zurich, PhD dissertation.
- Jiang, Q., 2019. Numerical simulations of solid-fluid coupling with dilated polyhedral DEM-SPH method based on GPU parallel algorithm. Dalian university of technology. Master thesis.
- Li, H., 2021. Numerical simulation of DEM-SPH coupling based on local average technique and parallel computation of GPU. Dalian university of technology. Master thesis.
- Liang, H., Jiang, Y., Ning, P., Zhu, L., 2023. A modified friction-viscous solid boundary of the SPH method for landslide simulation. *Comput. Geotech.* 155, 105238.
- Lin, C., Lin, M., 2015. Evolution of the large landslide induced by typhoon morakot: A case study in the butangbunasi river, southern taiwan using the discrete element method. *Eng. Geol.* 197, 172–187.
- Lo, C., Lin, M., Tang, C., et al., 2011. A kinematic model of the Hsiaolin landslide calibrated to the morphology of the landslide deposit. *Eng. Geol.* 123 (1–2), 22–39.
- Lobovský, L., Botia, E., Castellana, F., et al., 2014. Experimental investigation of dynamic pressure loads during dam break. *J. Fluid. Struct.* 48, 407–434.
- Ma, G., Kirby, J., Hsu, T., et al., 2015. A two-layer granular landslide model for tsunami wave generation: Theory and computation. *Ocean Model.* 93, 40–55.
- R.G. Mikola N., 2014. Sitar 3D Simulation of Tsunami Wave Induced by Rock Slope Failure Using Coupled DDA-SPH. proceedings of the 48th US Rock Mechanics/ Geomechanics Symposium, ARMA-2014-7094.
- Monaghan, J., 2005. Smoothed particle hydrodynamics. *Rep. Prog. Phys.* 68, 1703–1759.
- Morris, P., Fox, J., Zhu, Y., 1997. Modeling low Reynolds number incompressible flows using SPH. *J. Comput. Phys.* 136, 214–226.
- Panizzo, A., De, P., Di, M., et al., 2005. Great landslide events in Italian artificial reservoirs. *Nat. Hazards Earth Syst. Sci.* 5 (5), 733–740.
- Quecedo, M., Pastor, M., Herreros, I., 2004. Numerical modelling of impulse wave generated by fast landslides. *Int. J. Numer. Meth. Eng.* 59 (12), 1633–1656.
- Ren, S.P., Chen, X.J., Ren, Z.L., et al., 2023. Large-deformation modelling of earthquake-triggered landslides considering non-uniform soils with a stratigraphic dip. *Comput. Geotech.* 159, 105492.
- Robinson, M., Ramaoli, M., Luding, S., 2014. Fluid-particle flow simulations using two-way-coupled mesoscale SPH-DEM and validation. *Int. J. Multiph. Flow* 59 (2), 121–134.
- Serrano, P.A., Murillo, J., García, P., 2009. A finite volume method for the simulation of the waves generated by landslides. *J. Hydrol.* 373 (3), 273–289.
- Shan, T., Zhao, J., 2014. A coupled CFD-DEM analysis of granular flow impacting on a water reservoir. *Acta Mech.* 225 (8), 2449–2470.
- Sizkow, S.F., El Shamy, U., 2021. SPH-DEM simulations of saturated granular soils liquefaction incorporating particles of irregular shape. *Comput. Geotech.* 134, 104060.
- Sun, X., Sakai, M., Yamada, Y., 2013. Three-dimensional simulation of a solid-liquid flow by the DEM-SPH method. *J. Comput. Phys.* 248, 147–176.
- Tan, H., Chen, S., 2017. A hybrid DEM-SPH model for deformable landslide and its generated surge waves. *Adv. Water Resour.* 108, 256–276.
- Tang, L., Hu, C., Lin, L., et al., 2009. The Tsaojing landslide triggered by the chi-chi earthquake, taiwan: Insights from a discrete element simulation. *Eng. Geol.* 106 (1–2), 1–19.
- Tsuji, Y., Kawaguchi, T., Tanaka, T., 1993. Discrete particle simulation of two-dimensional fluidized bed. *Powder Technol.* 77 (1), 79–87.
- Viroulet, S., Sauret, A., Kimmoun, O., 2014. Tsunami generated by a granular collapse down a rough inclined plane. *EPL* 105 (3), 34004.
- Wang, W., Chen, Q., Zhang, H., et al., 2016. Analysis of landslide-generated impulsive waves using a coupled DDA-SPH method. *Eng. Anal. Bound. Elem.* 64, 267–277.
- Wendland, H., 1995. Piecewise polynomial, positive definite and compactly supported radial functions of minimal degree. *Adv. Comput. Math.* 4, 389–396.
- Xu, W.J., Dong, X.Y., 2021. Simulation and verification of landslide tsunamis using a 3D SPH-DEM coupling method. *Comput. Geotech.* 129, 103803.
- Yin, K., Du, J., Wang, Y., 2008. Analysis of surge triggered by dayantang landslide in shuibuya reservoir of qingjiang river. *Rock Soil Mech.* 29 (12), 3266–3270 in Chinese.
- Yin, Y., Huang, B., Chen, X., et al., 2015. Numerical analysis on wave generated by the Qianjiangping landslide in Three Gorges Reservoir. China. *Landslides.* 12 (2), 355–364.
- Zhang, G., Chen, J., Qi, Y., et al., 2022. A WCSPH two-phase mixture model for tsunami waves generated by granular landslides. *Comput. Geotech.* 144, 104657.
- Zhang, W., Wu, Z., Peng, C., et al., 2023. Modelling large-scale landslide using a GPU-accelerated 3D MPM with an efficient terrain contact algorithm. *Comput. Geotech.* 158, 105411.